Surface & Coatings Technology 268 (2015) 173–179

Contents lists available at ScienceDirect

Surface & Coatings Technology

journal homepage: www.elsevier.com/locate/surfcoat

Hardness of thermal sprayed coatings: Relevance of the scale of measurement

D. Chicot [a,*], H. Ageorges [c], M. Voda [d], G. Louis [e], M.A. Ben Dhia [c], C.C. Palacio [b,c], S. Kossman [a]

[a] Laboratoire de Mécanique de Lille, LML, UMR 8107, UST Lille, IUT A GMP, BP 90179, 59 653 Villeneuve d'Ascq, France
[b] Universidad EAFIT, Applied Electromagnetism Research Group, Cra. 49 No. 7 sur 50, Medellin, Colombia
[c] Centre Européen de la Céramique (CEC), Laboratoire Sciences des Procédés Céramiques et de Traitements de Surface (SPCTS), 12 rue Atlantis, 87068 Limoges, France
[d] "Politehnica" University of Timisoara, Mechanical Faculty, Bd. Mihai Viteazu Nr.1, Timisoara 300222, Romania
[e] Mines Douai, LGCgE, F-59500 Douai, France

ARTICLE INFO

Article history:
Received 20 January 2014
Accepted in revised form 23 April 2014
Available online 2 May 2014

Keywords:
Coating
Porosity
Roughness
Indentation
Hardness

ABSTRACT

The coatings obtained by thermal spraying can present a large variety of geometrical parameters (*thickness*, *roughness*…), of microstructures (*constituents*, *nature of phases*…), of mechanical properties (*hardness*, *elastic modulus*…) and of morphological defects (*cracks*, *pores*…) depending on the spraying conditions. In order to determine the mechanical properties of the coating, one of the most relevant techniques is probably the instrumented indentation test. Nowadays this technique is very attractive since it allows the determination of numerous parameters. Moreover, recent developments allow the use of a phenomenological approach and modeling at different scales of measurement, from nano (even ultra-nano) to macro scale, i.e. from few milligrams to several kilograms of loading. However, the information, which can be extracted at the different regimes of loading can be the same or lead to different values of the mechanical properties, which can be complementary or contradictory depending on the nature of the coating and the preparation of the sample. For example, roughness, porosity and cracks present in the coating will affect the mechanical characterization since the indentation data analysis is based on how a rigid indenter penetrates into the material. So, an important question arises: Should the influence of these defects to be taken into account, or neglected, for the mechanical characterization?

The present work proposes different methodologies for determining the hardness of coated materials by considering or not the influence of both the porosity and roughness of the surface. In the first part, results of microindentation experiments performed on the rough surface of alumina coatings are compared to those obtained on a polished cross-section. Although the surface of the cross-section is irregular even after caution polishing, the hardness can be measured. A decrease of about 30% of the hardness number on the cross-section is observed. The second part is related to the microstructured yttria-stabilized zirconia analysis. A methodology based on the indentation size effect analysis is presented to avoid the influence of roughness and the defects, which can be crossed by the indenter during the indentation. This methodology allows the hardness determination of the coating exempt of defects. In the last part, a statistical analysis using nanoindentation data resulting from the continuous stiffness measurement mode applied to nanostructured yttria-stabilized zirconia shows that, even if the hardness number varies to a great extent according to the applied load and the location of the indent, the hardness can be represented by means of a unique hardness number independent of the sense of the hardness variation during the indenter displacement.

© 2014 Elsevier B.V. All rights reserved.

1. Introduction

Thermal sprayed coatings are nowadays widely employed due to their large variety of geometrical and microstructural parameters like thickness, porosity, roughness, hard and soft phases, which could be present into the coating. These parameters are recognized to influence significantly the mechanical properties [1–3]. Therefore, their determination is necessary for studying the mechanical behavior of coated materials according to their usage [4]. Therefore, the researcher has to face some problems for determining the mechanical properties of the coating in relation to its heterogeneity, porosity content, roughness and the cracks network, all of which depend on the thermal spraying conditions [5,6].

Usually for mechanical characterization, the instrumented indentation test is employed since it allows the determination of a large variety

* Corresponding author at: IUT "A", CREST, Dpt Génie Mécanique et Productique, Rue de la Recherche, BP 90179, 59653 Villeneuve d'Ascq Cedex, France. Tel.: +33 359 572 852; fax: +33 320 677 321.
E-mail address: Didier.Chicot@univ-lille1.fr (D. Chicot).

http://dx.doi.org/10.1016/j.surfcoat.2014.04.043
0257-8972/© 2014 Elsevier B.V. All rights reserved.

of parameters like hardness [7,8], elastic modulus [7,8], indentation toughness [9], tensile properties [10], fatigue and creep behavior [11] and the interfacial indentation toughness [12] for characterizing the adhesion of a thick coating onto its substrate. Moreover, the materials can be studied at different scales of measurement, from nano to macroindentation, which renders this mechanical test very popular. As an example, nanoindentation is mostly used to study the mechanical properties of a particle, a local phase or a very thin film, whereas microindentation can give mechanical properties at an intermediate scale of measurement. On the other hand, macroindentation can be employed for characterizing the global behavior of a material since the material under indentation can be considered as to a homogeneous one. However, problems arise when studying rough and porous coatings. For such type of materials, nanoindentation is very sensitive to the roughness and the presence of pores under the indenter. Contrarily, macroindentation is less sensitive to porosity, but the results can be influenced by the presence of the substrate, which can interfere into the measurement. In this case, models for separating the influence of the substrate should be applied but their efficiency and accuracy must be considered. It seems that microindentation could be the most appropriate technique for analyzing such a coating even if the presence of pores and defects also modifies the indenter penetration way and, subsequently, the mechanical properties' determination.

In this work, we collect some results obtained on three thermal sprayed coatings presenting heterogeneity, roughness at the surface and pores in the coating. The microstructural analyses together with the mechanical characterization of these coatings are presented in three distinct sections. In the first section, we compare the hardness of an alumina coating deduced from microindentation tests performed at the top surface and on a cross-section. On the top surface in order to circumvent any change of the mechanical properties, no polishing has been conducted. Note that in this case, the origin of a load–displacement curve corresponds to the contact of the indenter with the material, which can be located at the top or in a hollow of the rough surface, thus leading inevitably to a discrepancy of the results. On the other hand, indentation tests have been performed using the same range of loads on a polished cross-section but the results equally show a large variation because the surface is not smooth enough even after polishing. In the second section concerning the analysis of an yttria-stabilized zirconia coating, we proposed a methodology, which allows the separation of the influence of roughness, which predominantly appears at the beginning of the loading and the influence of pores and cracks, which lead to a shift of the load–displacement curve toward the high depths when the indenter crosses the defect. This methodology is based on the analysis of the loading curve by means of the Proportional Specimen Resistance (PSR) model proposed by Li and Bradt [13] and the Strain Gradient Plasticity (SGP) model proposed by Nix and Gao, [14] afterwards extended by Chicot [15] for representing the indentation size effect equally at nano and micrometer regimes. The last section is devoted to the analysis of a nanostructured yttried zirconia coating. The hardness results from the continuous stiffness measurement mode in nanoindentation, which allows the plot of hardness versus the indenter displacement. In this situation, a statistical approach allows the determination of a representative hardness value. The different approaches presented here can be reasonably employed according to the scientific objective, i.e. obtaining the mechanical properties of the global coating, with or without the consideration of the defects, or the mechanical properties of a specific phase or particle.

2. Experiments

The hardness determination has been performed by instrumented indentation experiments both at a microscale and a nanoscale. The microindentation tests were performed with a micro-hardness Tester CSM 2-107 equipped with Vickers and Berkovich indenters. The maximum loads were chosen within the range 100 mN to 10 N and close to 50 indentation tests were randomly conducted at the top surface and on the cross-section of the coating. The indentation on the non-polished top surface of the coating has been motivated in order to avoid any modification of the microstructure and possible changes in the indentation data analysis, i.e. modification of the residual stress state, filling or plugging of the pores, generation of cracks and work-hardening. To study the influence of the preparation mode of the sample, hardness tests have been performed on a polished cross-section. The values of the loading and unloading rates (expressed in mN/min) were set at twice the value of the maximum applied load, according to the rule proposed by Quinn et al. [16]. A dwell-time of 15 s was imposed according to the standard indentation test procedure conducted in classical indentation tests according to the ASTM E92 and E384-10e2 standards.

Nanoindentation experiments have been conducted employing a Nano Indenter XP™ (MTS Nano Instruments) with a Berkovich indenter. 30 indentation tests have been conducted randomly at the surface of the polished coated system by applying the same indentation testing conditions. The maximum indentation depth reached by the indenter was fixed at 800 nm and the strain rate was equal to 0.05 s^{-1}. The instrument was operated in the Continuous Stiffness Measurement mode (CSM) allowing the determination of the hardness at each data point during the indentation loading. The harmonic displacement was 2 nm and the frequency is equal to 45 Hz. The sample was fixed on a metallic support using the heat softening glue crystal bond 509.

3. Results and discussion

3.1. Comparison between top surface and cross-section hardness determination of an Alumina coating

The alumina coating under investigation has been manufactured by Atmospheric Plasma Spraying (APS) with a conventional d.c. plasma gun PTF4 from Sulzer Metco. The powder used is α-Al_2O_3 agglomerated nanometric powder with a size ranging between 200 and 500 nm agglomerated into 25 to 100 μm (d_{50} = 55 μm) grain-size [17]. The powder is sprayed onto a low carbon steel (XC38) as substrate. The substrate was firstly grit blasted with corundum alumina then cleaned in an acetone bath with ultrasonic stirring before the spraying. The resulting roughness was 5.3 ± 0.1 μm. The anode nozzle diameter was 7 mm. The powder was injected perpendicularly to the plasma jet axis through a 1.8 mm i.d. injector located 3 mm upstream of the torch nozzle exit. The plasma jet parameters used are presented in Table 1.

The microstructure analysis of the coating was performed by X-ray Diffraction (XRD) for identifying the phases present into the coating and with a SEM-JEOL JSM-6490LV microscope to observe the microstructure and the defect distribution through the coating. The coating obtained with the agglomerated nanometric powder has a large surface mean roughness, Ra = 9.4 ± 1.8 μm. The XRD analysis using the SIEMENS D5000TM equipment shows that the coating is composed of both α and γ alumina phases, 81.8 and 18.2%, respectively. The SEM

Table 1
Plasma jet parameters used to obtain the Alumina sprayed coatings deposited onto a low carbon steel substrate.

Parameters	Unit	Value
Arc current	A	600
Voltage	V	65
Argon flow rate	slm	45
Hydrogen flow rate	slm	15
Spray distance	mm	100
Gun Traverse speed	m/s	1
Powder flow rate	g/min	25
Argon carrier gas flow rate	slm	5
Number of cycles	–	39
Spray time	min	4

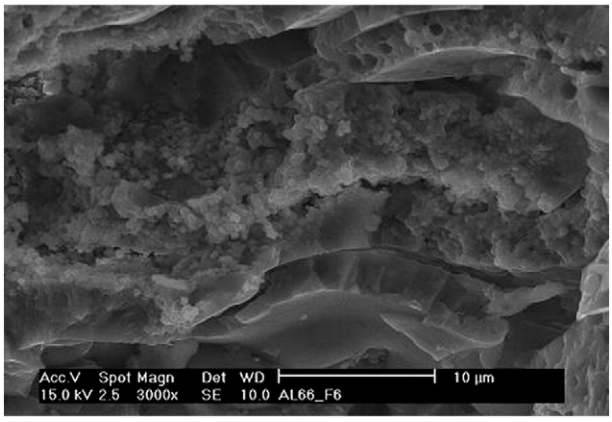

Fig. 1. SEM micrograph of the coating showing the bimodal structure of the alumina sprayed coating.

analysis shows that the coating presents a bimodal lamellar structure with non-melted nanometric particles embedded in melted lamellae characteristic of such coating (Fig. 1). This structure leads to inter-lamellar porosity associated to the intra-lamellar structure. The coating thickness is of 475 ± 25 µm, which allows neglecting the influence of the substrate in microindentation tests performed perpendicularly to the interface between the coating and the substrate.

In this study, we determined two hardness numbers: 1) the Martens Hardness, HM, equals to the ratio between the applied load and the true contact area calculated with the maximum indentation depth, which can be compared to classical Vickers hardness and 2) the contact hardness usually used in nanoindentation, H_{IT}, considering the projected contact area in the plane of the surface of the material calculated with the contact indentation depth, following the methodology proposed by Oliver and Pharr [7,8]. The Martens hardness and the contact hardness are expressed as follows:

$$HM = \frac{L}{26.43 \cdot h_m^2} \quad \text{and} \quad H_{IT} = \frac{L}{24.56 \cdot h_c^2} \tag{1}$$

where L is the indentation load in N, h_m is the maximum indentation depth and h_c is the contact depth both expressed in mm for obtaining a hardness number in MPa.

To obtain a representative hardness number, more than 50 indentation experiments have been performed randomly at the top surface of the non-polished coating. The two hardness numbers are presented as a function of the indentation depth on Fig. 2 where Fig. 2a reveals the important roughness of the coating.

Fig. 2b shows that the two hardness numbers, 16.6 ± 3 GPa for H_{IT} and 12.4 ± 3 GPa for HM, vary to a large extent due to the influence of roughness and the presence of defects into the coating. To study the influence of the hardness determination mode, a series of indentation tests have been performed on a cross-section cautiously polished for obtaining a mirror-like surface. Fig. 3a shows that the surface is not smooth enough as it could be expected. The roughness has not been reduced to less than 2.5 µm. In fact, the polishing highlights two different zones at the surface alternating smooth and uneven zones. As a result, the indents present irregular edges as well as some deflections and cracks in the neighborhood of the indent. Following the same methodology employed for characterizing the top surface, we have performed numerous indentation experiments randomly on the polished cross-section. Fig. 3b represents the two hardness numbers as a function of the reciprocal indenter displacement. We obtained 11.5 ± 2.3 GPa for H_{IT} and 7.8 ± 1.2 GPa for HM. It is noticeable that the standard deviation has not been significantly reduced after polishing as compared to the results obtained on the rough top-surface. This is due to the presence of hard phases mixed with softer phases with which the polishing led to irregular surfaces.

Additional classical Vickers hardness measurements have been performed on the polished cross-section using a load of 3 N during 15 s of dwell-time. The mean value of the microhardness, HV, resulting from 20 indents is about 7.5 ± 1.1 GPa, which is in a very good accordance with the Martens hardness, HM, thus confirming that Vickers and Martens hardness values can be reasonably compared.

As a conclusion, the indentation experiments on the cross-section have not allowed a better representation in terms of standard deviation of the hardness numbers as compared to those obtained at the top surface of the coating. Different causes due to the polishing or the microstructure of the coating could be at the origin of the hardness number decrease of about 30% as compared to the value obtained on the as-sprayed top surface. Indeed, the polishing could lead to a release of the residual stresses and/or to work hardening in a region very close to the polished zone. In addition, the anisotropy of thermal spray ceramic coatings namely interlamellar sliding may occur during indentation into the cross-section, which would explain why a lower hardness value is measured [18,19].

3.2. Separation of the material defects from the indentation data analysis on an Yttria-Stabilized Zirconia (YSZ) coating

This microstructured yttria-stabilized zirconia coating has been presented in [20]. This coating is produced from commercial powder

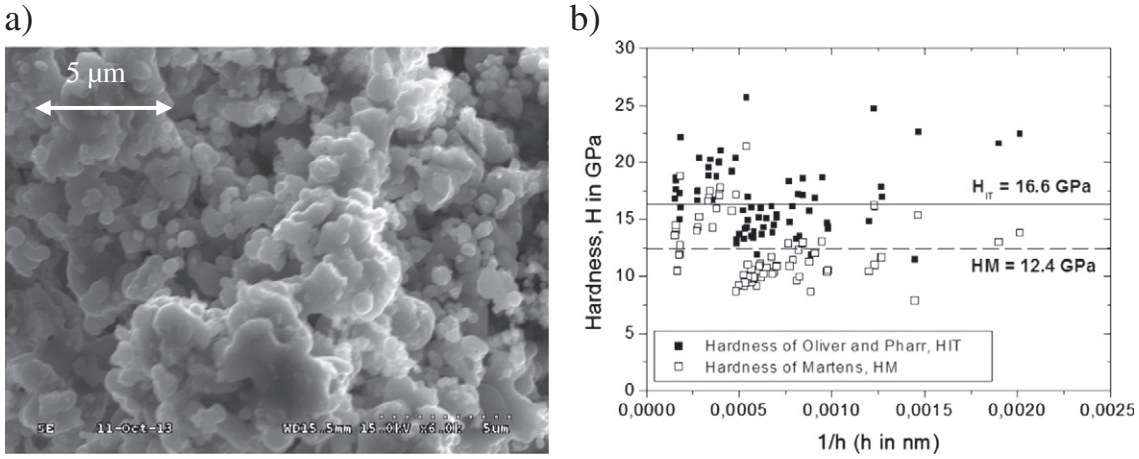

Fig. 2. (a) Top surface by SEM of the alumina coating and (b) corresponding hardness numbers (H_{IT} and HM) as a function of the reciprocal indenter displacement.

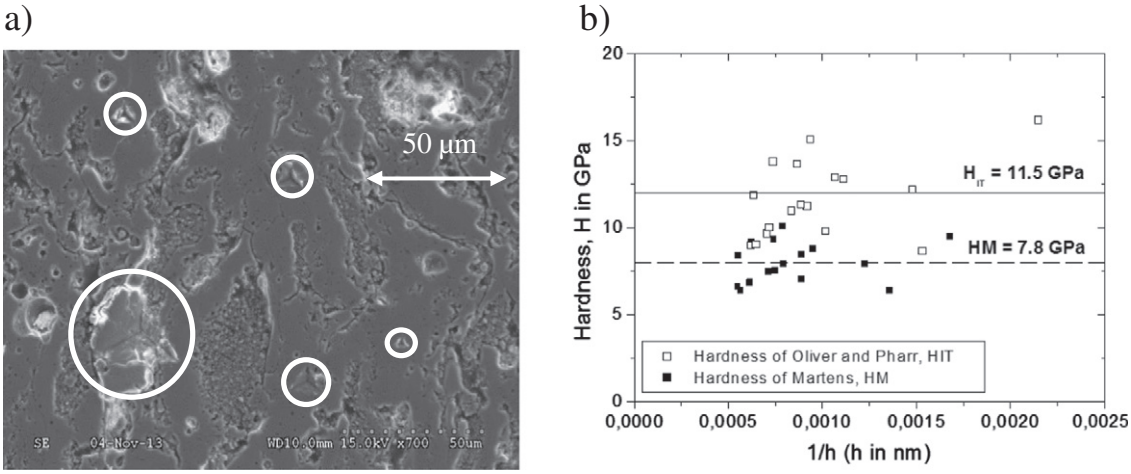

Fig. 3. (a) Cross-section by SEM of the alumina sprayed coating and (b) corresponding hardness numbers (H_{IT} and HM) as a function of the reciprocal indenter displacement.

Metco 204NS of fine particles with a composition of ZrO_2 + 8 wt.% Y_2O_3 and with a mean size of 4.6 μm and a monomodal size distribution. The suspension used for the spray experiments was formulated with the use of 20 wt.% of powder, 40 wt.% of water and 40 wt.% of ethanol. The suspension feed rate for the spray experiment was of about 39 g/min. The suspension was introduced via internal injection mode using a continuous-stream injector (with an internal diameter of 0.5 mm) installed inside the anode-nozzle of the plasma torch. Plasma spraying was performed using an *SG-100* (*Praxair S.T.*, Indianapolis, In, USA) d.c. single cathode torch mounted on a 5-axis *IRB-6* robot of *ABB* (Zürich, Switzerland) using an Ar + H_2 (45 + 5 slpm) plasma gas mixture with electric power of 40 kW. The suspension spraying was performed in order to obtain coatings with a thickness of up to 100 μm. Stainless steel disks (diameter 25 mm and thickness about 8 mm), initially cleaned with ethanol and sand blasted using corundum grit under a pressure of 0.04 MPa from a distance of 100 mm, were used as substrates.

The coatings were sprayed by applying 3 passes in one scan over the substrate, with a scan step of 10 mm. After each scan, the deposition was interrupted and the coatings were cooled down to about 60 °C. This experiment was made with a spray distance of 40 mm and a velocity of 300 mm/s. There were 6 sand blasted stainless steel substrates, which were sprayed simultaneously to obtain the desired thickness of about 100 μm. Fig. 4a and b shows the surface of the suspension plasma sprayed coatings. The figures reveal the presence of some micro-porosity and cracks at the top of the coating. It is also clear that the surface is heterogeneous according to the shape of the splats and that the size of the particles is randomly distributed at the surface of the coated sample.

Instrumented indentation in the micro-range of loads shows irregular load–displacement curves (Fig. 5). At the beginning of the loading, the shift toward the right of the figure is due to roughness and the changes occurring during loading are due to the presence of cracks and pores, which tends to increase the indenter penetration depth when it crosses through the defect. In addition to Malzbender and de With [21], who propose to model the loading curve for detecting the fracture of the coating, we suggest analyzing the loading curve to estimate the hardness of the coating.

It is clear that the hardness calculated at the maximum load, whatever the indenter displacement considered for its calculation, leads to a hardness value, which is not representative of the material since the shift toward the right observable at the beginning and during loading modifies the maximum penetration depth value, this diminishing the hardness number. That is why we calculated the hardness on the entire loading curve by considering each couple of load–depth data points [22]. This is only possible by considering the Martens hardness definition since the contact hardness is only accessible during the loading curve with the CSM mode. Additionally, in order to take into account the indentation size effect and for separating the influence of the roughness, we applied the methodology earlier proposed by Shen and Zeng, [23] who based their reasoning on the indentation size effect model developed by Li and Bradt [13]. These authors suggest expressing the

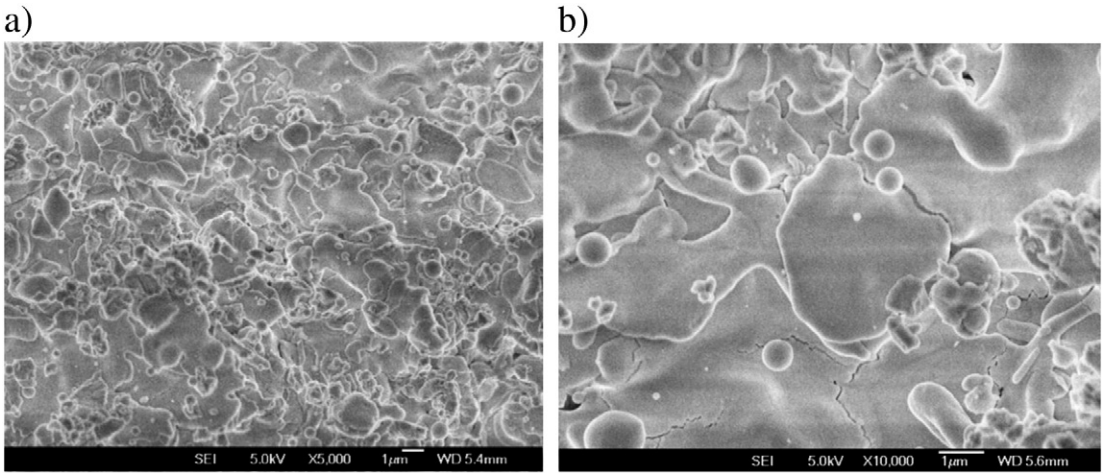

Fig. 4. SEM photo of the microstructured yttria-stabilized zirconia coating surface showing presence of pores, cracks and nodules, magnification 5000× (a) and 10,000× (b).

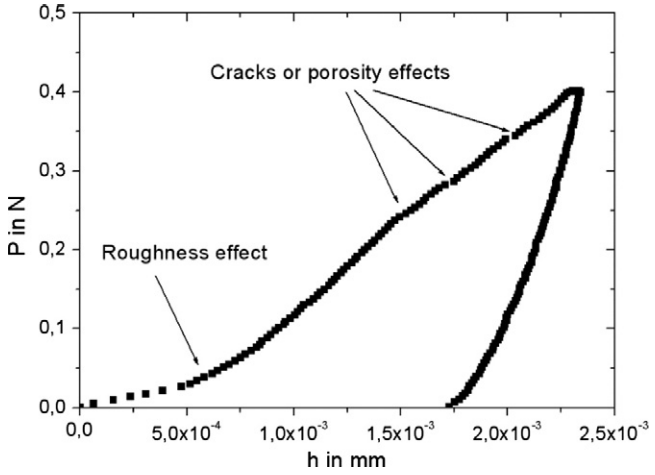

Fig. 5. Typical load–displacement curves obtained by the application of a Vickers indenter using 0.4 N of load applied onto the microstructured YSZ coating.

applied load as a function of the indentation depth according to the following polynomial law representing the Proportional Specimen Resistance (PSR) model:

$$P = C_0.h + C_1.h^2 \tag{2}$$

where C_0 and C_1 are constants which are material dependent and h represents the indentation depth.

Accordingly, the plot of (P/h) versus h must be represented by a straight line, whose intercept with the ordinate is C_0 and the slope C_1. The Martens hardness number is then expressed as a function of the two constants C_0 and C_1, which allows defining the Martens macrohardness, HM_0, and Δ, which represents the indentation size effect, as follows:

$$HM = HM_0 + \frac{\Delta}{h} \tag{3}$$

where HM_0 equals to $(C_1/26.43)$ and Δ to $(C_0/26.43)$.

Following this methodology, the loading curves are represented on Fig. 6a by plotting (P_i/h_i) as a function of (h_i). As it can be seen, the curves present distinct zones where the irregular zones correspond to the influence of the defects and the regular one the expected load–depth curves variation for a massive and homogeneous material. For the lowest values of (Pi/hi), the horizontal plateau is due to the roughness effect. The depth jumps observed for highest values of (Pi/hi) during the loading can be linked to the presence of voids, which consequently lead to a fast increase, or a jump, in depth. However, it is very interesting to note that the regular zone can be adequately represented by a straight line according to the model of Li and Bradt [7]. By analyzing various loading curves obtained under various maximum indentation loads, we obtained the mean values of 3.6 ± 1.1 GPa for HM_0 and of 0.2 ± 1.2 MPa m for Δ. This latest value has no real physical meaning since roughness influences its value as shown on Fig. 6a with the length of the horizontal plateau for the lowest values of the displacement.

Another approach consists in analyzing the indentation size effect by means of the strain gradient plasticity model proposed by Nix and Gao [14]. This model has been extended by Chicot [15], who proposed to express the Martens hardness as a function of the reciprocal indentation depth as follows:

$$HM^2 = HM_0^2 + \frac{H_{LSF}^2}{h} \tag{4}$$

where H_{LSF} is the hardness length-scale factor and h the indentation depth.

Note that in [15], H_{LSF} is expressed in MPa $m^{1/2}$, which is equivalent to a toughness. In this condition, this parameter could represent the resistance to plastic deformation by indentation. To model the load–depth curve, Chicot et al. [12] have proposed the calculation of the Martens hardness for a massive material employing the following relationship:

$$P = P_0 + 26.43 \cdot \left(HM_0^2 + \frac{H_{LSF}^2}{h}\right)^{1/2} \cdot h^2 \tag{5}$$

where three constants are involved: (i) the deviation load P_0, (ii) the dynamic Martens macrohardness HM_0, and, (iii) the hardness length-scale factor H_{LSF} representing the ISE of the material, as indicated in Eq. (4).

To take into account the influence of roughness at low loads, this relation must be adapted by introducing a shift in depth as follows:

$$P = 26.43 \cdot \left(HM_0^2 + \frac{H_{LSF}^2}{(h-h_0)}\right)^{1/2} \cdot (h-h_0)^2 \tag{6}$$

where the zero shift P_0 of Eq. (5) is replaced here by the shift in depth h_0.

Fig. 6b shows the fitting curve of a loading curve by applying Eq. (6). This methodology allows the separation of the roughness influence by

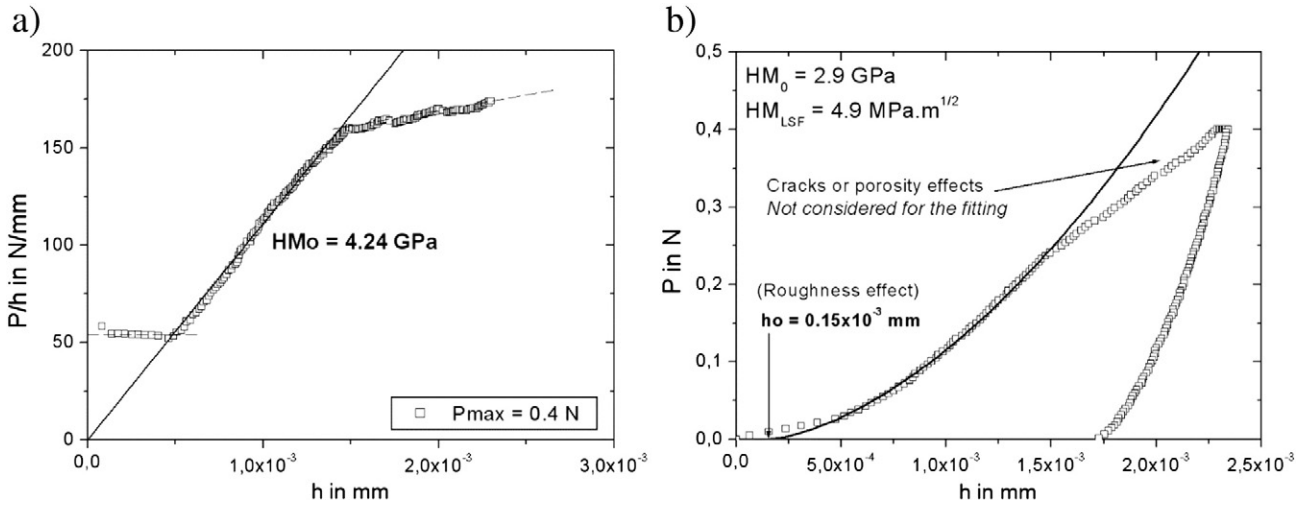

Fig. 6. (a) PSR model and (b) SGP model for representing the loading curve and calculating the macrohardness representative of the hardness of the microstructured YSZ coating.

Table 2
Suspension plasma spraying (SPS) parameters used to obtain nanostructured sprayed YSZ coating on Haynes substrate.

Parameters	Unit	Value
Plasma torch		F4-VB Sulzer-Metco
Anode diameter	mm	6
Plasma gas		Ar/He/H_2
Plasma gas flow rate	slm	45/45/3
Arc current	A	700
Liquid pressure	bar	3.2
Nozzle diameter	μm	250
Spray distance	mm	40
Plasma gun traverse speed	m/s	1.5
Plasma gun scanning step	mm	5
Deposition cycles 75 μm		150
Pre-heating temperature substrate	°C	400

introducing the shift in depth, h_0, and by neglecting influence of voids or pores by considering only the regular part of the loading curve. By applying this methodology over all the loading curves, we calculate the mean value of HM_0 which is equal to 3.5 ± 0.8 GPa and of H_{LSF} equal to 4.2 ± 1.0 MPa $m^{1/2}$.

3.3. Statistical analysis of indentation data performed on nanostructured Yttried Stabilized Zirconia coating

The nanostructured YSZ coating was deposited by suspension plasma spraying using 8YSZ (ZrO_2-8 mol% Y_2O_3) nanometric powders of particle size from 30 to 60 nm, provided by Inframat Corp. (Willington, CT, USA) and distilled water as solvent. The suspension was mixed by mechanical and ultrasonic stirring to break up the agglomerates without dispersants. The concentration of solid particles in the suspension was 6% wt. The thickness of the coating was 75 μm and the corresponding spray parameters are shown in Table 2.

Circular samples of Haynes 230 (Ni 57%, Cr 22%, W 14%, Mo 2%, and Fe max. 3%) as substrate having 30 mm in diameter and 3 mm in thickness were employed. Before the spraying, the substrate was ultrasonically cleaned by acetone and alcohol without any prior grit blasting. The average roughness of the substrate before deposition was 0.9 ± 0.2 μm. No metallic bond coat was used between the substrate and the nanostructured YSZ coating. SEM observations of the top surface (Fig. 7a) and cross-section (Fig. 7b) of the coating show that the coating exhibits a granular morphology formed by stacked grains. Some columnar stacking defects are also noticed from the fractography presented in Fig. 7b.

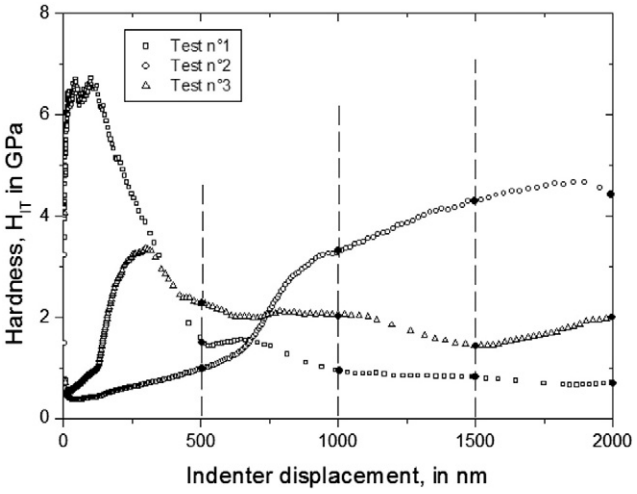

Fig. 8. Examples of variations of the hardness H_{IT} versus the indenter displacement for the YSZ coating.

For characterizing the mechanical behavior of such nanostructured coating, the indentation experiments have been carried out on the polished as-sprayed YSZ coating surface. The nanoindentation tests have been performed by applying the continuous stiffness measurement mode, which allows the plot of the hardness H_{IT} versus the indenter displacement. In this case, the hardness H_{IT} is calculated by dividing the applied load by the contact area taking into account the projected contact area and the contact depth, as defined by Oliver and Pharr [7, 8] in Eq. (1). Consequently, the value of H_{IT} cannot be compared to the Martens hardness since their definitions are completely different. This representation allows the correlation of the hardness changes with the crossing of a soft phase or a hard particle by the indenter. As an example, Fig. 8 shows some typical hardness-indenter displacement curves.

It is noticeable that the hardness number varies to a large extent with the indenter displacement, which is due to the heterogeneity of the coating in terms of porosity. If the material is dense very close to the top surface, the hardness has a high value around that observed by Vert et al. [24] for YSZ coating. As it can be seen on Fig. 8, when the indenter encounters a pore during its displacement, the apparent H_{IT}

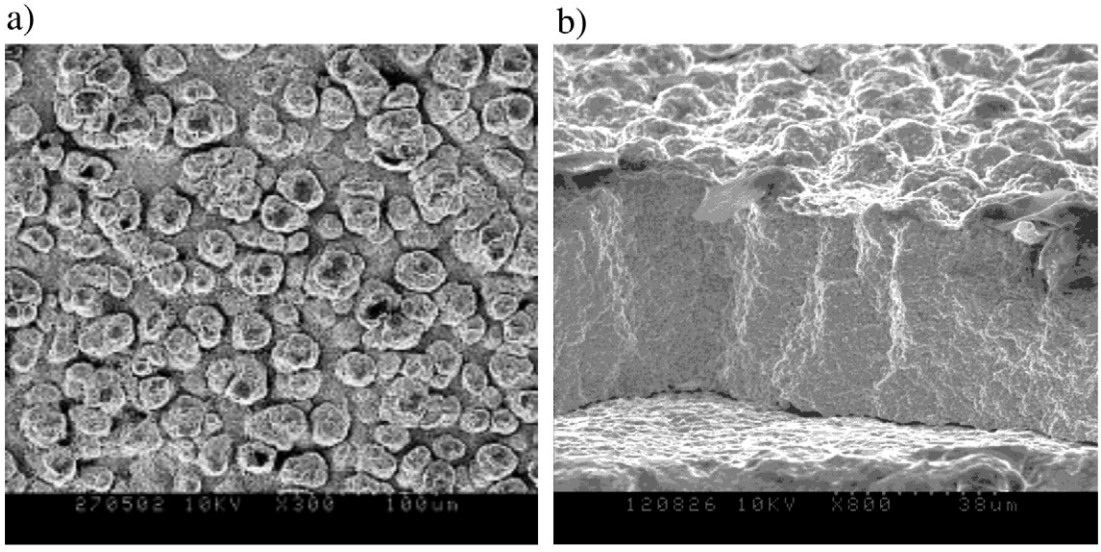

Fig. 7. Nanostructured YSZ coating, a) top surface and b) cross-section obtained after fracture.

Table 3
Hardness H_{IT} as a function of the indenter displacement.

h (nm)	500	1000	1500	2000
H_{IT} (GPa)	3.0 ± 2.1	2.4 ± 1.5	1.9 ± 1.0	1.8 ± 1.0

hardness value decreases at a high rate (case of test n° 1 in Fig. 8). Contrarily, if a pore is very close to the external surface of the material, the hardness has a very low value (case of test n° 2 and 3 in Fig. 8). Between these two extreme situations, the hardness versus displacement curve can take different shapes according to the quantity and size of the defects located in the neighborhood of the indent. Accordingly, an increase or decrease of the hardness number will take place. In these conditions, the analysis of the real mechanical behavior of the coating requires a cautious methodology. To circumvent such amplitude of variation, we proposed the calculation of a hardness number at a given indenter displacement, i.e. 500, 1000, 1500 and 2000 nm, as indicated in Fig. 8. Subsequently, we present in Table 3 the mean value and the standard deviation.

It is very interesting to note that the hardness value slightly decreases when the indenter displacement increases, which could be associated to an indentation size effect (ISE). Concerning the decrease of both the average hardness and standard deviation as the indentation depth increases, Nohava et al. [25,26] have observed similar phenomena on thermal sprayed coatings. The variation of the standard deviation shows that the material is strongly heterogeneous and that the measurement of the mechanical parameters strongly depends on the porosity of the coating and the location of the indentation test. In addition, Nohava et al. [25,26] have observed the formation of cracks and of collapsed voids in the neighborhood of the indent due to the application of higher indentation loads. A similar phenomenon has been observed by Malzbender and Steinbrech [27]. For these authors, the relative crack density in the deformed volume and the stiffness stress dependence due to crack closure are responsible of the hardness decrease.

4. Conclusions

Hardness determination greatly depends on the roughness of the outer surface of the coating and the presence of pores and/or cracks into the coating. In this paper, we have presented different methodologies, which allow taking into account their influences on the mechanical characterization:

1) On an alumina coating, we showed that a cautious polishing of the cross-section always lead to alternatively uneven and smooth surfaces, which clearly impede obtaining a constant hardness value of the coating. On the as-sprayed coating, the hardness number is found to be 30% higher than the value obtained on the cross-section. In addition, the standard deviation has been found to be of the same order of magnitude, with and without polishing of the surface to be analyzed. So, the decrease of the hardness number must be attributed to the microstructural changes resulting from the cutting and the polishing process.
2) To circumvent the influence of roughness and porosity on the hardness determination of the microstructured yttria-stabilized zirconia coating, we proposed a methodology consisting of analyzing the regular part of the loading curve by means of the proportional specimen resistance model and/or the strain gradient plasticity model. This latter model has been modified by introducing a corrective term representative of the shift at the origin due to the influence of roughness. Independent on the model applied, we showed that the macrohardness has the same value, but the parameter related to the indentation size effect takes a value which is not representative of the real indentation size effect since roughness greatly influences its determination. In addition we noted that the influence of cracks is represented by a shift of the loading curve toward higher depth values. After the crossing of a pore by the indenter, the loading curve shows the same form like before the crossing, thus confirming a continuity during the loading.
3) Another approach consists of a statistical analysis of the nanoindentation data obtained randomly on the surface of a nanostructured yttria-stabilized zirconia coating. The hardness variation versus the indenter displacement shows a large standard deviation due to the fact that the indenter crosses a hard particle, a soft matrix or a mixture of the two. The average hardness number is found to decrease slightly when the indenter displacement increases in relation to the microstructure change through the coating and/or the formation of cracks and collapsed voids around the indent.

As a conclusion, it is difficult to state what would be the best hardness measurement to represent the mechanical behavior of a specific material in relation to its application, design, behavior assessment and lifetime prediction. One of the main problems related to the hardness calculation is the definition of the contact area between the indenter and the material, i.e. the projected one or the actual contact area, the maximum indenter displacement or the contact depth. In addition, the indentation size effect must be taken into account but until today, a question arises on its origin: it is a real physical meaning or an artifact like the influence of the tip defect of the indenter. Afterwards, even if a methodology is selected to calculate the hardness number, should the influence of porosity, roughness, and cracks… be taken into account in the hardness characterization? The answer to this question would be related to the objective of the designer.

References

[1] M.S. Bobji, S.K. Biswas, Tribol. Lett. 7 (1999) 51–56.
[2] L. Hemmouche, D. Chicot, A. Amrouche, A. Iost, M.A. Belouchrani, X. Decoopman, G. Louis, E.S. Puchi-Cabrera, Mater. Sci. Eng. A 585 (2013) 155–164.
[3] A. Rico, M.A. Garrido, E. Otero, J. Rodríguez, Key Eng. Mater. 333 (2007) 247–250.
[4] A. Leyland, A. Matthews, Wear 246 (2000) 1–11.
[5] G. Shanmugavelayutham, A. Kobayashi, Trans. JWRI 34 (2005) N°1.
[6] O. Sarikaya, Surf. Coat. Technol. 190 (2005) 388–393.
[7] W.C. Oliver, G.M. Pharr, J. Mater. Res. 7 (1992) 1564–1580.
[8] W.C. Oliver, G.M. Pharr, J. Mater. Res. 19 (2004) 3–20.
[9] D. Chicot, G. Duarte, A. Tricoteaux, B. Jorgowski, A. Leriche, J. Lesage, Mater. Sci. Eng. A 527 (2009) 65–76.
[10] M. Yetna N'Jock, D. Chicot, X. Decoopman, J. Lesage, J.M. Ndjaka, A. Pertuz, Int. J. Mech. Sci. 75 (2013) 257–264.
[11] D. Chicot, K. Tilkin, K. Jankowski, A. Wymysłowski, Microelectron. Reliab. 53 (2013) 761–766.
[12] D. Chicot, P. Démarécaux, J. Lesage, Thin Solid Films 283 (1996) 151–157.
[13] H. Li, R.C. Bradt, Mater. Res. 28 (1993) 917–926.
[14] W.D. Nix, H. Gao, J. Mech. Phys. Solids 46 (1998) 411–425.
[15] D. Chicot, Mater. Sci. Eng. A 499 (2009) 454–461.
[16] G.D. Quinn, P.L. Patel, I. Lloyd, J. Res. Natl. Inst. Stand. Technol. 107 (2002) 299–306.
[17] H. Ageorges, R. Vert, G. Darut, F. Zishuan, in: B.R. Marple, M.M. Hyland, Y.C. Lau, C.J. Li, R.S. Lima, G. Montavon (Eds.), International Thermal Spray Conference & Exposition 2009 (ITSC2009): Expanding Thermal Spray Performance to New Markets and Applications, Las Vegas, USA, May 4–7 2009, ASM International, Materials Park, Ohio (USA), 2009, pp. 1195–1200, (CD-Rom).
[18] R.J. Damani, A. Wanner, J. Mater. Sci. 35 (2000) 4307–4318.
[19] R.S. Lima, S.E. Kruger, B.R. Marple, Surf. Coat. Technol. 202 (2008) 3643–3652.
[20] L. Łatka, D. Chicot, A. Cattini, L. Pawłowski, A. Ambroziak, Surf. Coat. Technol. 220 (2013) 131–139.
[21] J. Malzbender, G. de With, Surf. Coat. Technol. 137 (2001) 72–76.
[22] D. Chicot, D. Mercier, Mech. Mater. 40 (4–5) (2008) 171–182.
[23] L. Shen, K. Zeng, Microelectron. Eng. 71 (2004) 221–228.
[24] R. Vert, D. Chicot, C. Dublanche-Tixier, E. Meillot, A. Vardelle, G. Mariaux, Surf. Coat. Technol. 205 (2010) 999–1003.
[25] J. Nohava, R. Mušálek, J. Matějíček, M. Vilémová, Surf. Coat. Technol. 240 (2014) 243–249.
[26] J. Nohava, B. Bonferroni, G. Bolelli, L. Lusvarghi, Surf. Coat. Technol. 205 (2010) 1127–1131.
[27] J. Malzbender, R.W. Steinbrech, J. Mater. Res. 18 (2003) 1975–1984.